Quantitative Raman Spectrum and Reliable Thickness Identification for Atomic Layers on Insulating Substrates

Song-Lin Li,[†,‡,*] Hisao Miyazaki,[†] Haisheng Song,[†] Hiromi Kuramochi,[†] Shu Nakaharai,[§] and Kazuhito Tsukagoshi[†,*]

[†]WPI Center for Materials Nanoarchitechtonics (WPI-MANA) and [‡]International Center for Young Scientist (ICYS), National Institute for Materials Science, Tsukuba, Ibaraki 305-0044, Japan and [§]Collaborative Research Team, Green Nanoelectronics Center, National Institute of Advanced Industrial Science and Technology, Tsukuba, Ibaraki 305-8569, Japan

ABSTRACT We demonstrate the possibility in quantifying the Raman intensities for both specimen and substrate layers in a common stacked experimental configuration and, consequently, propose a general and rapid thickness identification technique for atomic-scale layers on dielectric substrates. Unprecedentedly wide-range Raman data for atomically flat MoS_2 flakes are collected to compare with theoretical models. We reveal that all intensity features can be accurately captured when including optical interference effect. Surprisingly, we find that even freely suspended chalcogenide few-layer flakes have a stronger Raman response than that from the bulk phase. Importantly, despite the oscillating intensity of specimen spectrum *versus* thickness, the substrate weighted spectral intensity becomes monotonic. Combined with its sensitivity to specimen thickness, we suggest this quantity can be used to rapidly determine the accurate thickness for atomic layers.

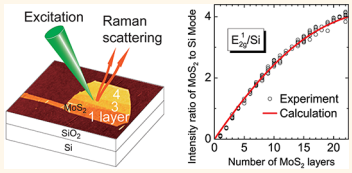

KEYWORDS: nanomaterial · atomic layer · Raman enhancement · characterization

Atomically thin two-dimensional (2D) crystals, including graphene,[1] exfoliated chalcogenides,[2,3] self-organized nanosheets,[4,5] and topological insulators,[6,7] have generated intensive research due to their scientific significance and technological potential. Stemming from drastic dimension reduction, numerous intriguing phenomena are observed, such as Dirac dispersion relation,[1,6,7] variable band structure,[8−10] and helical Dirac fermions.[6] For these materials, interesting phenomena are not necessarily limited in monolayer flakes and, sometimes, attractive properties emerge in samples with increased thickness. For instance, the surface state induced Dirac cones develop only in Bi_2Se_3 films thicker than five quintuple layers,[7] while under perpendicular electric field, energy gaps, form in bilayer rather than monolayer graphene.[11] Accurate thickness information and sufficient characterization range is particularly important for the ultrathin materials. So far, however, there have been few rapid and nondestructive thickness characterization techniques for the inorganic atomic layers. A direct transfer of the well established schemes from graphene, such as optical contrast[12,13] and Raman phonon position,[14,15] to the inorganic flakes seems not so successful. For example, the optical contrast exhibits a nonmonotonic response and a low sensitivity for few-layer chalcogenide flakes in most illumination wavelengths,[12] which largely reduces the convenience of use. Developing a general and effective thickness characterization scheme represents a strong desire from the scientific community.

On the other hand, it is well recognized that the optical interference has a strong impact on the intensity of the Raman spectrum.[16−19] This phenomenon draws renewed attention[20−22] after the isolation of the 2D graphene in 2004. In an important advance, Wang *et al.* first point out that the multiple reflections within the graphene and dielectric layers are responsible for the strong modulated Raman response at varied graphene thicknesses.[20] However, a discrepancy still exists between experiment and calculation, which could be understood as experimental errors due to inevitable interfacial roughness before 2004, but is hard to accept presently when atomically flat graphene flakes are used. This leaves a doubt whether there are other factors, such as surface plasmon,[23] involved in the Raman process. To solve this issue and strictly verify the interference effect on the Raman spectrum, an independent study on other materials is highly desired.

* Address correspondence to li.songlin@nims.go.jp, tsukagoshi.kazuhito@nims.go.jp.

Received for review June 7, 2012 and accepted July 28, 2012.

Published online July 28, 2012
10.1021/nn3025173

Propelled by the two motivations above, we performed an unprecedented Raman investigation on atomically flat MoS_2 flakes over a wide range from 1 to ~120 consecutive layers. We demonstrated that optical interference is the dominant factor affecting spectral response and managed to quantify the Raman intensities for both the MoS_2 specimen and Si substrate layers in the common stacked sample configuration. Excellent agreements between the interference-based models[21,22] and calculated data were achieved. In addition, by extracting the ratio of spectral intensity of MoS_2 to Si, we showed that this intensity ratio is a monotonic spectral invariant *versus* specimen thickness and is capable of identifying MoS_2 thickness. By appropriately incorporating the interference effect, strong responses (2−20-fold with respect to bulks) can be achieved from the atomic layers, no matter if they are freely suspended or supported by substrates. Raman spectra for other chalcogenides were also calculated and showed similar behavior as MoS_2, indicating a good generalization of above results. These results enable a quantitative understanding on Raman spectroscopy that may lead to versatile applications, such as rational design for Raman enhancement and thickness characterization for ultrathin structures.

RESULTS AND DISCUSSION

The chalcogenide MoS_2, an important electronic material—next generation graphene,[24,25] is chosen as the specimen because of its marked cleavage properties and potential applications in short-channel transistors[2,26−28] and optoelectronic components.[29] Interestingly, when thinned from bulk to monolayer, its band structure undergoes an indirect to direct change and the photoluminescence efficiency increases accordingly.[8−10] Besides, the energy gap and phonon modes also depend on the number of layers (NL).[14] The structure of the 2H-MoS_2 chalcogenides (space group: $P6_3/mmc$) is illustrated in Figure 1a, in which one cation (Mo^{4+}) plane is sandwiched between two anion (S^{2-}) planes and the layered structure arises from the stacking of hexagonally packed sheets in sequence.[30] Figure 1b,c shows optical and atomic force microscopy (AFM) images for MoS_2 flakes from consecutive 1−4 layers. In our AFM measurements, the tapping mode was employed to minimize sample damage. Figure 1d shows the average profile of the rectangular area presented in Figure 1c. The linear fit of the layer heights (Figure 1e) reveals a fake height of ~1.3 nm for bare SiO_2/Si substrates, which may arise from the different tapping responses of substrate and MoS_2, and a step height of 0.70 nm between consecutive layers, which is slightly larger than the theoretical value of 0.615 nm.[30] The NL values from 1 to 3 were determined from the distance of the Raman modes of E^1_{2g} and A_{1g} (Figure 2e), which is more accurate than AFM, while the values for NL > 3 are assigned through

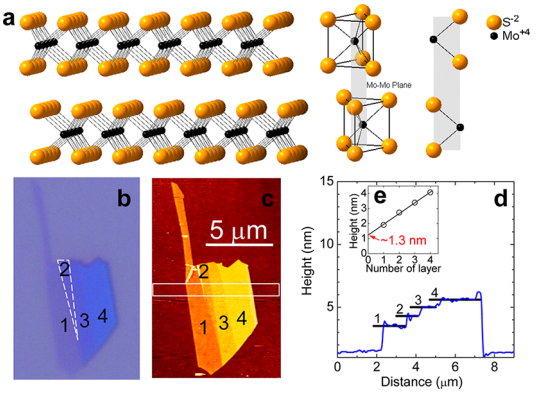

Figure 1. Atomic structure and characterization of ultrathin 2H-MoS_2 layers. (a) Atomic structure of 2H-MoS_2. (b, c) Typical optical and AFM images for an exfoliated MoS_2 flake with consecutive NL values from 1 to 4. (d) Average height profile for the rectangular area shown in (c). (e) Linear fit of the layer heights from 1 to 4 layers, which gives a base height of ~1.3 nm for the bare SiO_2/Si substrates and a step height of 0.70 nm between the consecutive layers.

combined AFM measurement and optical contrast, which brings out 10% error in the "nominal" NL values of our flakes. Raman spectra were taken for consecutive MoS_2 flakes and over a wide NL range from 1 to ~120 layers.

One of the reasons for extending Raman measurements to thick flakes is to determine the critical thickness for dimensionality crossover from 3D to 2D. Figure 2a shows typical Raman spectra for different NL values, and the spectral information (peak position, area, height, and width) is extracted with Lorentzian fittings. Two sharp Raman modes, E^1_{2g} (~383 cm^{-1}) and A_{1g} (~408 cm^{-1}), are observed and they exhibit strong NL dependence. The first decreases from 386 to 383 cm^{-1} and the second increases from 404 to 408 cm^{-1} as NL increases from 1 to 20 (Figure 2b,c), consistent with the observation of Lee *et al.*[14] These shifts are attributed to the variation in the dielectric screening environment for long-range Coulomb interactions as NL changes.[31] In addition to the above first-order modes, a rather weak second-order scattering process, 2 × LA(*M*) mode,[32] near 452 cm^{-1} was recorded. This mode is also NL-dependent, increasing from 447 to 452 cm^{-1}. Figure 2b−e reveals that the 3D properties for the lattice phonon modes of MoS_2 persist to a thickness of at least 10 layers and the 2D properties become essential as NL < 5.

An important finding here is the observation of an interference-induced high-order Raman enhancement peak, which was never seen in analogue systems.[14,20] Due to the narrow NL range covered in previous studies, only one enhancement peak is observed at NL ~ 10 in graphene[20] and at NL ~ 4 in MoS_2.[14] It is generally believed that no additional local maxima exist in thicker layers.[20] However, we identify a new enhancement peak at NL ~ 85 in MoS_2. In Figure 2f,g, the multiple enhancement peaks manifest themselves

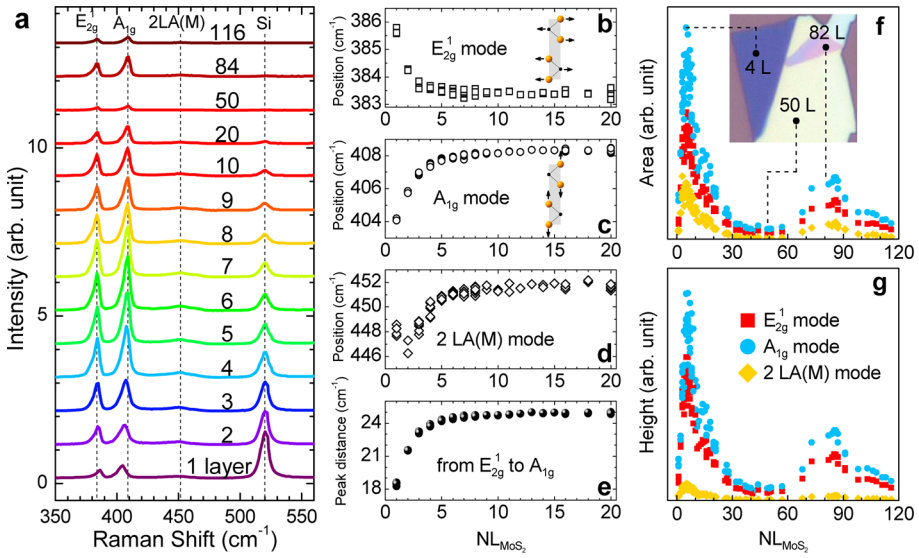

Figure 2. Raman spectra for MoS_2 flakes and evolution of spectral features with thickness. (a) Typical Raman spectra of MoS_2 flakes at different NL values from 1 to 116. (b−d) Position evolution for the three Raman modes E^1_{2g}, A_{1g}, and 2 × LA(*M*) as a function of NL. (e) Peak distance between the E^1_{2g} and A_{1g} modes. (f) Area and (g) height plots for the three modes as a function of NL. The inset of (f) is an optical image for an MoS_2 flake of three typical NL values (4, 50, and 82).

as two intensity maxima when plotting peak area and height as a function of NL. All three Raman modes exhibit the same intensity tendency, indicating that this enhancement effect is independent of the lattice vibration modes. The colors of the MoS_2 flakes are also suggestive of the interference effect. Under white light illumination, the flakes with thickness near the first and second peaks are dark blue and pink, respectively, while the flake with a thickness around the first valley exhibits a dim white color (inset of Figure 2f).

As mentioned, although efforts have been made in understanding the spectral response as a function of graphene thickness,[20] a large discrepancy remains between the calculation and experiment. The most important contribution here is accurately quantifying the Raman spectra over a wide NL range, which allows us to rule out the possibility of other factors, such as surface plasmon,[23] engaging in the Raman process so that we can draw an affirmative conclusion that optical interference is the sole modulation source. Note that strict optical relations for three-layer systems are quite complicated.[18,19] Similar to previous works,[20,21] a simplification made here is only the normal incidence considered so that the p- and s-components of excitation can share the same expression in calculation. We also checked that such a simplification would not cause a large deviation, because most additional contributions due to oblique incidence cancel out between p- and s-components and the majority of light is close to normal incidence condition due to the Gaussian distribution of laser energy (section 3, Supporting Information). As will be seen below, this first-order approximation catches the main experimental features and gives a satisfied accuracy to fit with experiment.

The optical paths for the excitation and scattering light are quite complex because the incident light undergoes an infinite number of reflections and refractions at the boundaries of both MoS_2 and SiO_2 layers (Figure 3a). A strategy for solving this optical issue is to first calculate the effective reflection coefficient at the MoS_2/SiO_2 interface by accounting for multiple reflections in the SiO_2 dielectric layer and then analyze the light distribution in the MoS_2 specimen layer.[20] For convenience, the four involved media are designated by the index *i*, and the corresponding complex refractive indices are represented by $\tilde{n}_i$, where $i = 0$, 1, 2, and 3 for air, MoS_2, SiO_2, and Si, respectively. After including the multiple reflections, the output Raman intensity from the top MoS_2 layer (total thickness d_1) can be expressed as[21]

$$I = \int_0^{d1} |F_{ex}(x)F_{sc}(x)|^2 dx \qquad (1)$$

where $F_{ex}(x)$ and $F_{sc}(x)$ are the electric field amplitudes for the excitation and scattering light, respectively. The derivation and the full expressions of them are given in sections 1.1−1.3 in the Supporting Information.

Figure 3b compares the calculation and experiment for the E^1_{2g} mode at varied NL values. The calculation agrees well with the experiment in terms of the peak positions and the spectral intensity from 4 to 120 layers. For instance, it duplicates the two peak positions at NL ∼ 4 and 80 and their intensity ratio of ∼3. Such an excellent agreement is rather surprising because the current calculation contains no fitting parameters. This agreement also unambiguously indicates the exclusive modulation role played by optical interference in the stacked systems. For NL < 4, reduced Raman responses are observed, which can be attributed to the decreased real thickness of few-layer flakes compared with the theoretical values we adopted in

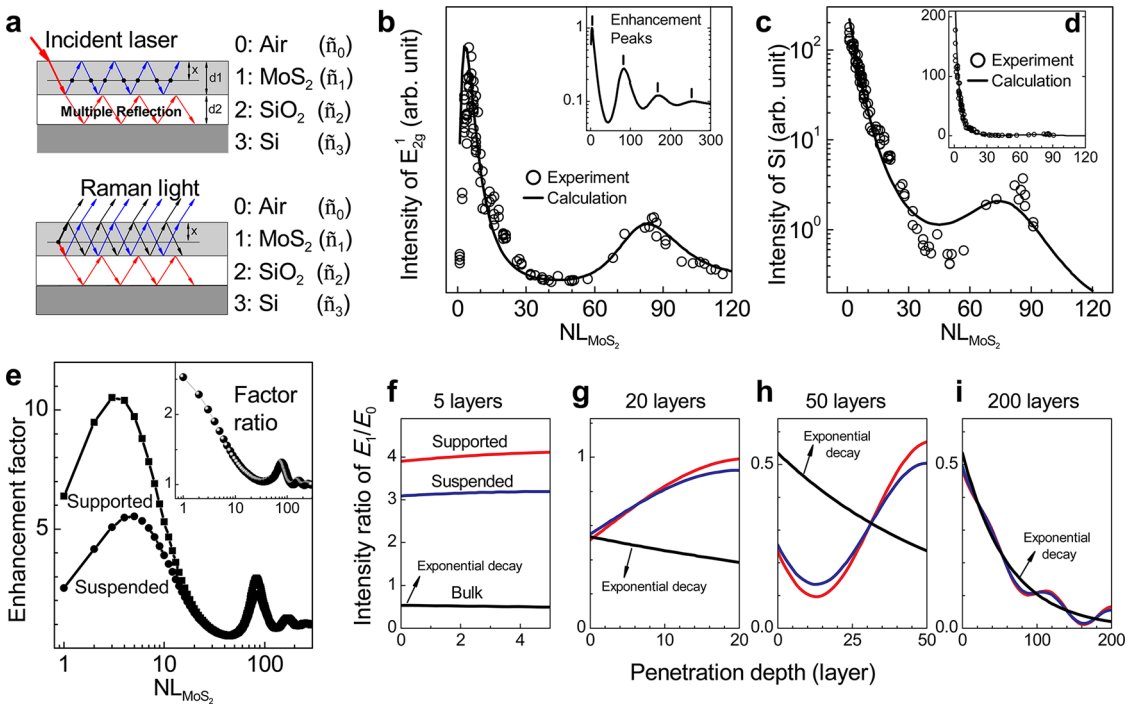

Figure 3. Modeling and comparison between calculation and experiment for the thickness-dependent spectral intensities in the $MoS_2/SiO_2/Si$ stack. (a) Schematic diagrams for the optical paths of the excitation and Raman scattering light, respectively. (b) Calculation and experiment for the MoS_2 layers at different NL values. (c, d) The corresponding results for the Si substrate, plotted in logarithmic and linear scales, respectively. (e) Calculated enhancement factor for suspended and supported (on 285 nm SiO_2) MoS_2 flakes of different thicknesses. The inset is the corresponding factor ratio for the two geometries. (f−i) Distribution of excitation light within MoS_2 flakes of selected NL values of 5, 20, 50, and 200 layers. For the bulk, the intensity of the excitation light follows a exponential decay with a starting intensity $\sim 0.5|E_0|^2$. The low initial value is due to the low light transmissivity from air to MoS_2 ($|t_{01}|^2 = |2\tilde{n}_0/(\tilde{n}_0 + \tilde{n}_1)|^2 \sim 0.1$).

calculation by using the integer times of layer spacing in bulk. The phenomenon of thickness reduction is common in ultrathin materials and was reported in graphene and nanotube systems.[33] Extending the calculation to a large NL regime reveals the existence of four enhancement peaks within 300 layers. Their enhancement factors (relative to bulk) decay from 10, 3.0, and 1.3 to 1.1. For NL > 300, no clear enhancement peak exists. In addition to the enhancement peaks from constructive interference, valleys due to destructive interference are also observed. The intensity of the first valley at NL ∼ 45 is only half of the bulk value. The presence of both constructive peaks and destructive valleys further confirms the interferential nature of the observed spectra.

The accurate control on the specimen thickness also enables an interesting observation on the modulation pattern of the Raman spectrum of substrate layer. Actually, in the $MoS_2/SiO_2/Si$ stack, the response from the Si substrate at 520 cm^{-1} is not only rather strong but also close to the two MoS_2 main modes of E^1_{2g} and A_{1g} (Figure 2a). The three peaks are inevitably recorded together during collection. An analysis on the "byproduct" of Si peak also helps to check the validity of established interference model. Here we find that besides the specimen spectrum, the interference model describes the substrate spectrum as well. The related derivation and expression for the Si spectrum can be found in section 1.4 in the Supporting Information. In Figure 3d, the calculated spectrum *versus* NL of MoS_2 is plotted and characterized by a dominant exponential decay, which results from the strong absorption of incident light by the MoS_2 layer above SiO_2. The interferential feature from the Si spectrum is not as appreciable as the MoS_2 spectrum, but still discernible at NL ∼ 80 when plotted the intensity logarithmically in Figure 3c. The successful duplication of the weak fine structures confirms again the validity of established interference models.

A surprising finding in this work is that a MoS_2 monolayer, no matter freely suspended or placed above SiO_2, can have stronger Raman response than bulks. This strikingly contradicts the intuition that atomic layers would have much weak signals due to the drastic amount reduction. Figure 3e shows the enhancement factor for the suspended and supported MoS_2 flakes with respect to bulks. We choose the bulk phase as reference because such a configuration excludes all interference paths and corresponding spectrum is easy to obtain. For a monolayer, the enhancement factors reach 2.5 and 6 in the suspended and supported configurations, respectively. The highest enhancement factor for freely suspended MoS_2 flakes is 5 at NL ∼ 4, while the value doubles when

an additional 285 nm SiO_2 layer is employed as an interference enhancement layer.

To understand this phenomenon, the intensity distributions of excitation light within the MoS_2 flakes are calculated under different specimen configurations. For the bulk configuration, the light follows a traditional light absorption process, that is, an exponential decay from incident position. The initial intensity relates to transmittance coefficient t_{01} (from air to MoS_2) and is calculated to be $\sim 0.5|E_0|^2$, where $|E_0|^2$ is the intensity of excitation laser. For freely suspended and supported five layers, the intensities are almost fixed at $\sim 3|E_0|^2$ and $4|E_0|^2$, respectively, both higher than that in the bulk configuration (Figure 3f). This theoretical result thus provides a fundamental support for investigating the intrinsic spectral behavior for freely suspended samples.[34] Additionally, the light distributions in the suspended and supported configurations are highly dependent on NL, controlled by the two processes of optical absorption and interference (Figures 3g–i). When NL > 200, the distributions in the two configurations approach that in the bulk.

Another essential motivation of this work is to develop a general and rapid criterion for counting NL for atomic inorganic flakes. The full quantification on spectral behavior enables us to reach the goal by using the intensity ratio of MoS_2 to Si as the criterion (Figure 4), as was done in graphene.[22] In calculating the intensity ratios, the scattering cross sections for the MoS_2 E^1_{2g} and A_{1g} modes were taken as 2.3 and 3.9 times of that of Si substrate, respectively. It is evident that, despite the oscillating intensity of the MoS_2 spectrum (Figure 2f), the weighted intensity by Si spectrum becomes monotonic for all NL range (inset of Figure 4b), making it rival the previous optical contrast method.[12,13] As shown in Figure 4a,b, both the E^1_{2g} and A_{1g} modes can be used and the most sensitive range spans from 1 to 20 layers. This new criterion, in principle, covers all NL range. Its limitation to large NL regime stems from the fast decay in the Si spectrum and the increasing fitting uncertainties (Figure 3d). For less absorbed specimens, the detection range is expected to extend. Error analysis is also performed for this identification method and shown in Figure 4c,d. For NL ≤ 7, the intensity ratios are discrete enough to discern each NL values, while the error is one layer in the 7 < NL < 15 regime and increases to two layers in the NL > 15 regime. The overall error is concluded to be ±10% for the investigated range. Nevertheless, the 20-layer detection ability and ±10% thickness accuracy are sufficient in most cases for the low-dimensional studies on atomic layers. The intensity ratio for varied SiO_2 thicknesses is also calculated and given in Figure 4e,f. Sufficient detection resolutions are disclosed when the SiO_2 thickness is changed by ±30 nm around optimal values of 91 and 273 nm. It deserves noting that to achieve excellent identification resolutions

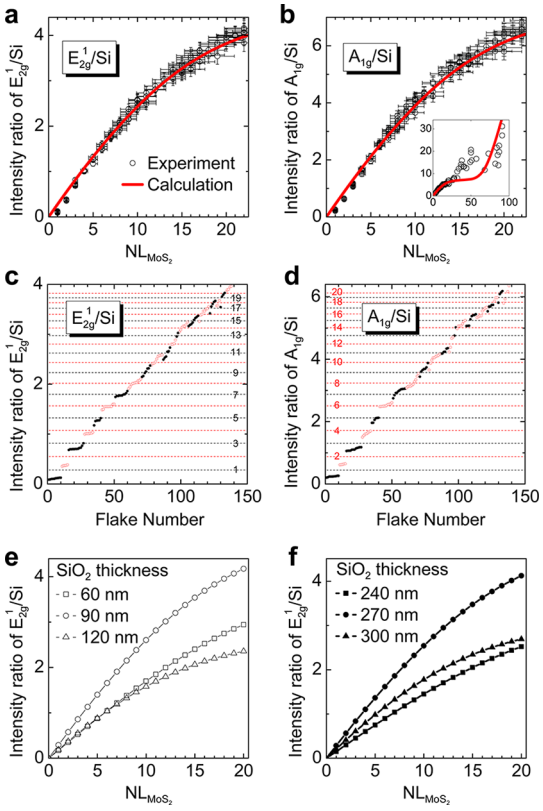

Figure 4. (a–d) Comparison between the calculation and experiment for the intensity ratio of the MoS_2 E^1_{2g} (~383 cm^{-1}) and A_{1g} (~408 cm^{-1}) modes to that of the Si substrate (520 cm^{-1}). The errors for the assigned NL values and intensity ratios are 10 and 5%, respectively. (e, f) Calculated intensity ratios at different SiO_2 thicknesses around optimal values of 91 and 273 nm.

some specific SiO_2 thickness ranges that cause destructive interference should be avoided, as will be discussed later.

To fully understand the spectrum for rational designs for Raman enhancement, we further calculated the dependence of the spectral intensity on three main experimental factors: the NL of MoS_2 (NL_{MoS_2}), the SiO_2 thickness (d_2), and the excitation wavelength (λ_{ex}). Figure 5a shows a contour plot of the enhancement factor (excited at 532 nm) as a function of NL_{MoS_2} and d_2. The irregular traces of the constructive peaks (dotted lines) are characteristic of the roles played by NL_{MoS_2} and d_2 in the interference phase factor $\phi = 2\pi\tilde{n}_1 d_1/\lambda_{ex} + 2\pi\tilde{n}_2 d_2/\lambda_{ex}$. When NL_{MoS_2} ($\propto d_1$) increases, d_2 has to decrease to maintain the constructive condition, $\phi = (N + 1/2)\pi$ (N = integer). This provides a basic reference in optimizing dielectric thickness for detecting atomic layers. As far as monolayers are concerned, the optimal SiO_2 thickness is $d_2 \sim (2N + 1)\lambda_{ex}/4n_2$. An enlarged plot for the ultrathin range (1–20 layers) is given in Figure 5b. The horizontal axis is reduced to the period factor $2n_2d_2/\lambda_{ex}$ to eliminate explicit experimental parameters. The maximum enhancement factors range from 3 to 14 (inset of Figure 5b). It is also

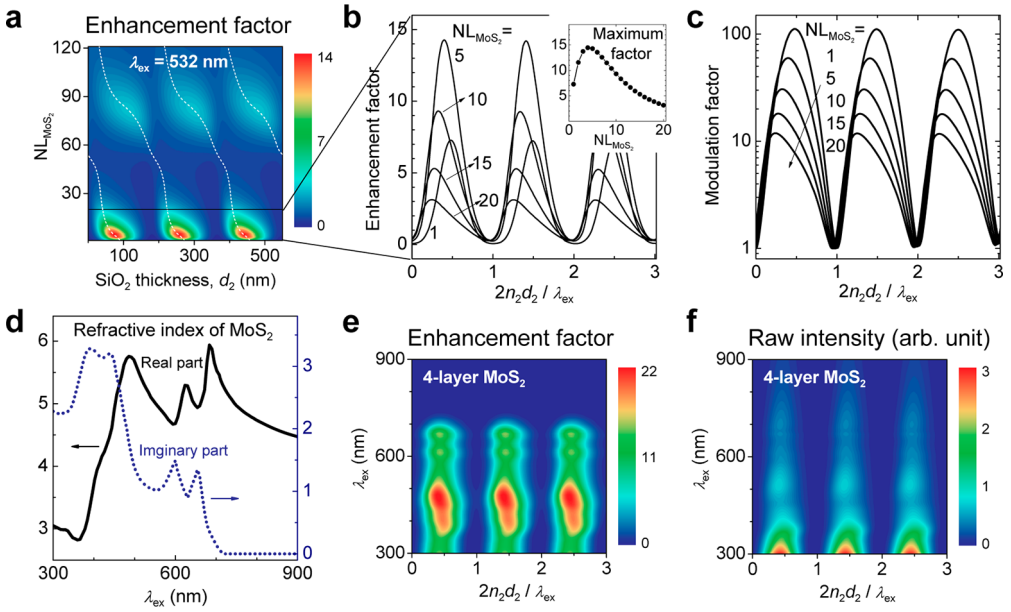

Figure 5. Dependence of spectral characteristics on three experimental factors: the NL of MoS_2 (NL_{MoS_2}), the SiO_2 thickness (d_2), and the excitation wavelength (λ_{ex}). (a) Contour plot of the calculated enhancement factor as a function of NL_{MoS_2} and d_2 at λ_{ex} = 532 nm. (b) Enlarged plot for low NL regime for typical NL_{MoS_2} values of 1, 5, 10, 15, and 20. (c) Corresponding modulation factor for (b), which is normalized to spectral minimum and reflects the intensity variation due to the change of the SiO_2 thickness d_2. (d) Highly dispersive refractive index of MoS_2. (e) Enhancement factor as a function of λ_{ex} and $2n_2d_2/\lambda_{ex}$ for a 4-layer MoS_2. The highest value reaches 22. (f) Corresponding raw spectral intensity for (e). The strongest response appears at high-frequency regime due to the well-known quartic relation between scattering cross section and excitation frequency.

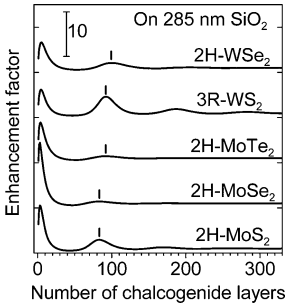

Figure 6. Calculated enhancement factor for five important layered chalcogenides, MoS_2, $MoSe_2$, $MoTe_2$, WS_2, and WSe_2, on 285 nm SiO_2/Si substrates under a 532 nm excitation. The curves are shifted for clarity. The vertical bars indicate the second enhancement peaks for a guide of eyes.

important to keep in mind the existence of destructive interference when inappropriate dielectric thicknesses are used, which would lead to a reduction in spectral intensity by 1−2 orders of magnitude (Figure 5c). Therefore, a careful thickness arrangement on specimen and dielectric is necessary.

When calculating the wavelength dependence, special attention was paid to the dispersion of refractive indices ($\tilde{n} = n - ik$) with wavelength, as well as the well-known quartic dependence of scattering cross section on excitation frequency $\sigma \propto f^4$. The n and k values of MoS_2 (and other four chalcogenides) from 300 to 900 nm excitation are explicitly given in Figure 5d (and Figures S4−S7, Supporting Information), which may be useful for future studies. The enhancement factor exhibits oscillating patterns with respect to the phase factor $2n_2d_2/\lambda_{ex}$. Its magnitude is highly dependent on the combination of n and k values, with the highest value reaching 22 near 490 nm (Figure 5e). At $\lambda_{ex} > 700$ nm, the factor approaches zero, resulting from the largely increased bulk response due to the reduction in light absorption in the long-wavelength regime ($k \sim 0$, Figure 5d). High raw intensity is located in the high-frequency regime due to the quartic dependence of scattering cross section on frequency (Figure 5f), indicating that high-frequency excitation helps to obtain a strong response.

Additional efforts were made to calculate the spectra for the other four chalcogenides, $MoSe_2$, $MoTe_2$, WS_2, and WSe_2 (Figures S4−S7), because they may contribute to ultrathin-channel electronics as MoS_2. The NL-dependent enhancement factor for the E^1_{2g} modes are shown in Figure 6. In low NL regime, all of the five materials have a stronger first-order Raman response than corresponding bulks with an enhancement factor from 2 to 15, which suggests that a sole interference enhancement is enough to achieve sufficient Raman signals for these atomic layers. Second-order enhancement peaks appear in all materials, but with distributed intensities. The position of the second enhancement peak follows the sequence $MoS_2 < MoSe_2 < WS_2 < MoTe_2 < WSe_2$, in line with the magnitude of the real part n in their refractive indices (Table S2, Supporting Information). Normally, high-order peaks are strong in materials with small k (imaginary part of refractive index) and large n values, such as WS_2 and MoS_2. This is because

a small k results in low sample absorption and large interferential components, and a large n leads to a short optical path required for interference and thus reduces absorption. Both factors are beneficial for light interference and final peak intensity. This understanding enables the recheck of the situation in graphene, which has a refractive index around $2.66-1.33i$, being small n and large k values as compared with chalcogenides. Therefore, its high-order enhancement peaks are not strong (Figure S2, Supporting Information) and tend to be hidden in noise during measurements. This result explains why multiple enhancement peaks are hard to be observed in graphene.[20]

CONCLUSION

We have conducted extensive measurements and calculations on the Raman spectra of chalcogenide flakes on dielectric substrates. For the first time, we observe clear high-order enhancement peaks in atomically flat samples and reveal the decisive role played by optical interference in the spectra of stacked systems. Impressively, quantitative Raman spectra are achieved in a wide range for both the specimen and the substrate layers. We also reveal that even freely suspended few-layer flakes can have stronger response than bulks due to inner optical interference. Besides rational designs for Raman enhancement, we also lay an important theoretical foundation for a thickness identification technique for inorganic atomic layers. The results provide insightful view in the Raman behavior of common stacked systems and would lead to versatile applications.

EXPERIMENTAL SECTION

MoS_2 flakes were prepared by micromechanical cleavage from commercial MoS_2 crystals (Furuchi, Japan) and were transferred to Si wafers with a 285 nm SiO_2 capping layer. Hybrid techniques of Raman peak position, AFM, and optical contrast spectra were used to determine the NL values for MoS_2 flakes. Raman spectra were acquired at an excitation wavelength of 532 nm and a laser power of less than 0.1 mW to avoid sample heating or oxidation in air. An integration time of 30 s was used to enhance the signal-to-noise ratio. The laser beam was focused onto the MoS_2 sample by a 100× objective lens with an NA of 0.9. The scattered light was collected and collimated by the same lens. The scattered signal was dispersed by a spectrometer working at 1800 grooves/mm and was detected by a thermoelectrically cooled CCD (charge-coupled device) detector at −60 °C. The spectral resolution was 0.7 cm^{-1}. All of the Raman spectra were recorded for the same integration time, laser power, and focus status. The size of focused beam was about 1 μm and only flakes larger than 2 μm were used. To avoid edge and corner effect, all spectra were collected by carefully focusing the beam spot to one layer without overlapping neighboring layers. However, MoS_2 flakes typically have a degraded uniformity and smaller sample area as compared with graphene. The flakes with close NL values are hard to identify under optical microscopy in the NL > 7 regime. Although we try to focus incident laser on uniform MoS_2 flakes, the results still contain data from nonuniform flakes. This brings about uncertainties when identifying thick samples. The 520 cm^{-1} Si first-order Raman mode was used for calibration.

In theoretical calculations, the refractive index values of Si and SiO_2 were adopted from literature.[35,36] The real (n) and imaginary (k) parts in refractive index of chalcogenides were translated from the corresponding dielectric permittivity and absorption coefficients,[37,38] and the accurate $\tilde{n}$ values at specific wavelength were obtained by data interpolation.

Conflict of Interest: The authors declare no competing financial interest.

Supporting Information Available: The expression derivation of Raman scattering for a trilayer system, the Raman response of graphene/graphite, the MoS_2 spectrum with objective lens of varied NA values, the calculated spectra for other chalcogenides, the calculated values of intensity ratios for NL identification, and the refractive indices used in the calculations for the four involved optical media. This material is available free of charge *via* the Internet at http://pubs.acs.org.

Acknowledgment. This work was supported in part by a Grant-in-Aid for Scientific Research (No. 21241038) from the Ministry of Education, Culture, Sports, Science and Technology of Japan and by the FIRST Program from the Japan Society for the Promotion of Science.

Note Added after ASAP Publication: After this paper was published online August 2, 2012, a correction was made to the name of the first author, Song-Lin Li. The corrected version was reposted August 15, 2012.

REFERENCES AND NOTES

1. Novoselov, K.; Geim, A.; Morozov, S.; Jiang, D.; Zhang, Y.; Dubonos, S.; Grigorieva, I.; Firsov, A. Electric Field Effect in Atomically Thin Carbon Films. *Science* **2004**, *306*, 666–669.
2. Radisavljevic, B.; Radenovic, A.; Brivio, J.; Giacometti, V.; Kis, A. Single-Layer MoS_2 Transistors. *Nat. Nanotechnol.* **2011**, *6*, 147–150.
3. Coleman, J. N.; Lotya, M.; O'Neill, A.; Bergin, S. D.; King, P. J.; Khan, U.; Young, K.; Gaucher, A.; De, S.; Smith, R. J.; et al. Two-Dimensional Nanosheets Produced by Liquid Exfoliation of Layered Materials. *Science* **2011**, *331*, 568–571.
4. Mitzi, D.; Kosbar, L.; Murray, C.; Copel, M.; Afzali, A. High-Mobility Ultrathin Semiconducting Films Prepared by Spin Coating. *Nature* **2004**, *428*, 299–303.
5. Schliehe, C.; Juarez, B. H.; Pelletier, M.; Jander, S.; Greshnykh, D.; Nagel, M.; Meyer, A.; Foerster, S.; Kornowski, A.; Klinke, C.; et al. Ultrathin PbS Sheets by Two-Dimensional Oriented Attachments. *Science* **2010**, *329*, 550–553.
6. Hsieh, D.; Xia, Y.; Qian, D.; Wray, L.; Dil, J. H.; Meier, F.; Osterwalder, J.; Patthey, L.; Checkelsky, J. G.; Ong, N. P. et al. A Tunable Topological Insulator in the Spin Helical Dirac Transport Regime. *Nature* **2009**, *460*, 1101–1105.
7. Zhang, Y.; He, K.; Chang, C.-Z.; Song, C.-L.; Wang, L.-L.; Chen, X.; Jia, J.-F.; Fang, Z.; Dai, X.; Shan, W.-Y.; et al. Crossover of the Three-Dimensional Topological Insulator Bi_2Se_3 to the Two-Dimensional Limit. *Nat. Phys.* **2010**, *6*, 584–588.
8. Eda, G.; Yamaguchi, H.; Voiry, D.; Fujita, T.; Chen, M.; Chhowalla, M. Photoluminescence from Chemically Exfoliated MoS_2. *Nano Lett.* **2011**, *11*, 5111–5116.
9. Mak, K. F.; Lee, C.; Hone, J.; Shan, J.; Heinz, T. F. Atomically Thin MoS_2: A New Direct-Gap Semiconductor. *Phys. Rev. Lett.* **2010**, *105*, 136805.
10. Splendiani, A.; Sun, L.; Zhang, Y.; Li, T.; Kim, J.; Chim, C.-Y.; Galli, G.; Wang, F. Emerging Photoluminescence in Monolayer MoS_2. *Nano Lett.* **2010**, *10*, 1271–1275.
11. Li, S.-L.; Miyazaki, H.; Hiura, H.; Liu, C.; Tsukagoshi, K. Enhanced Logic Performance with Semiconducting Bilayer Graphene Channels. *ACS Nano* **2011**, *5*, 500–506.

12. Castellanos-Gomez, A.; Agraït, N.; Rubio-Bollinger, G. Optical Identification of Atomically Thin Dichalcogenide Crystals. *Appl. Phys. Lett.* **2010**, *96*, 213116.
13. Late, D. J.; Liu, B.; Matte, H. S. S. R.; Rao, C. N. R.; Dravid, V. P. Rapid Characterization of Ultrathin Layers of Chalcogenides on SiO_2/Si Substrates. *Adv. Funct. Mater.* **2012**, *22*, 1894–1905.
14. Lee, C.; Yan, H.; Brus, L. E.; Heinz, T. F.; Hone, J.; Ryu, S. Anomalous Lattice Vibrations of Single- and Few-Layer MoS_2. *ACS Nano* **2010**, *4*, 2695–2700.
15. Zhang, J.; Peng, Z.; Soni, A.; Zhao, Y.; Xiong, Y.; Peng, B.; Wang, J.; Dresselhaus, M. S.; Xiong, Q. Raman Spectroscopy of Few-Quintuple Layer Topological Insulator Bi_2Se_3 Nanoplatelets. *Nano Lett.* **2011**, *11*, 2407–2414.
16. Nemanich, R. J.; Tsai, C. C.; Connell, G. A. N. Interference-Enhanced Raman Scattering of Very Thin Titanium and Titanium Oxide Films. *Phys. Rev. Lett.* **1980**, *44*, 273–276.
17. DiLella, D. P.; Gohin, A.; Lipson, R. H.; McBreen, P.; Moskovits, M. Enhanced Raman Spectroscopy of CO Adsorbed on Vapor-Deposited Silver. *J. Chem. Phys.* **1980**, *73*, 4282–4295.
18. Ager, J. W., III; Veirs, D. K.; Rosenblatt, G. M. Raman Intensities and Interference Effects for Thin Films Adsorbed on Metals. *J. Chem. Phys.* **1990**, *92*, 2067–2076.
19. Blue, D.; Helwig, K.; Moskovits, M.; Wolkow, R. Interference Effects in Surface Enhanced Raman-Scattering by Thin Adsorbed Layers. *J. Chem. Phys.* **1990**, *92*, 4600–4608.
20. Wang, Y. Y.; Ni, Z. H.; Shen, Z. X.; Wang, H. M.; Wu, Y. H. Interference Enhancement of Raman Signal of Graphene. *Appl. Phys. Lett.* **2008**, *92*, 043121.
21. Yoon, D.; Moon, H.; Son, Y.-W.; Choi, J. S.; Park, B. H.; Cha, Y. H.; Kim, Y. D.; Cheong, H. Interference Effect on Raman Spectrum of Graphene on SiO_2/Si. *Phys. Rev. B* **2009**, *80*, 125422.
22. Koh, Y. K.; Bae, M.-H.; Cahill, D. G.; Pop, E. Reliably Counting Atomic Planes of Few-Layer Graphene ($n > 4$). *ACS Nano* **2011**, *5*, 269–274.
23. Zhou, W.; Lee, J.; Nanda, J.; Pantelides, S. T.; Pennycook, S. J.; Idrobo, J.-C. Atomically Localized Plasmon Enhancement in Monolayer Graphene. *Nat. Nanotechnol.* **2012**, *7*, 161–165.
24. Mas-Balleste, R.; Gomez-Navarro, C.; Gomez-Herrero, J.; Zamora, F. 2D Materials: To Graphene and Beyond. *Nanoscale* **2011**, *3*, 20–30.
25. Neto, A. H. C.; Novoselov, K. New Directions in Science and Technology: Two-Dimensional Crystals. *Rep. Prog. Phys.* **2011**, *74*, 082501.
26. Frank, D.; Taur, Y.; Wong, H.-S. Generalized Scale Length for Two-Dimensional Effects in MOSFETs. *IEEE Electron Device Lett.* **1998**, *19*, 385–387.
27. Liu, L.; Kumar, S. B.; Ouyang, Y.; Guo, J. Performance Limits of Monolayer Transition Metal Dichalcogenide Transistors. *IEEE Trans. Electron Devices* **2011**, *58*, 3042–3047.
28. Yoon, Y.; Ganapathi, K.; Salahuddin, S. How Good Can Monolayer MoS_2 Transistors Be? *Nano Lett.* **2011**, *11*, 3768–3773.
29. Yin, Z.; Li, H.; Li, H.; Jiang, L.; Shi, Y.; Sun, Y.; Lu, G.; Zhang, Q.; Chen, X.; Zhang, H. Single-Layer MoS_2 Phototransistors. *ACS Nano* **2012**, *6*, 74–80.
30. Wilson, J. A.; Yoffe, A. D. The Transition Metal Dichalcogenides Discussion and Interpretation of Observed Optical, Electrical and Structural Properties. *Adv. Phys.* **1969**, *18*, 193–335.
31. Molina-Sanchez, A.; Wirtz, L. Phonons in Single-Layer and Few-Layer MoS_2 and WS_2. *Phys. Rev. B* **2011**, *84*, 155413.
32. Frey, G. L.; Tenne, R.; Matthews, M. J.; Dresselhaus, M. S.; Dresselhaus, G. Raman and Resonance Raman Investigation of MoS_2 Nanoparticles. *Phys. Rev. B* **1999**, *60*, 2883–2892.
33. Huang, Y.; Wu, J.; Hwang, K. C. Thickness of Graphene and Single-Wall Carbon Nanotubes. *Phys. Rev. B* **2006**, *74*, 245413.
34. Berciaud, S.; Ryu, S.; Brus, L. E.; Heinz, T. F. Probing the Intrinsic Properties of Exfoliated Graphene: Raman Spectroscopy of Free-Standing Monolayers. *Nano Lett.* **2009**, *9*, 346–352.
35. Edwards, D. F. Silicon (Si). In *Handbook of Optical Constants of Solids*; Palik, E. D., Ed.; Academic Press: San Diego, 1985; Vol. 1, pp 564–565.
36. Philipp, H. R. Silicon Dioxide (SiO_2) (Glass). In *Handbook of Optical Constants of Solids*; Palik, E. D., Ed.; Academic Press: San Diego, 1985; Vol. 1, p 760.
37. Beal, A. R.; Hughes, H. P. Kramers-Kronig Analysis of the Reflectivity Spectra of 2H-MoS_2, 2H-$MoSe_2$ and 2H-$MoTe_2$. *J. Phys. C: Solid State Phys.* **1979**, *12*, 881.
38. Beal, A. R.; Liang, W. Y.; Hughes, H. P. Kramers-Kronig Analysis of the Reflectivity Spectra of 3R-WS_2 and 2H-WSe_2. *J. Phys. C: Solid State Phys.* **1976**, *9*, 2449.